



Design of Optimal Parameter for Solid-State Welding of EN 10028-P355 GH Steel Using gray Incidence Reinforced Response Surface Methodology

G. Senthilkumar¹ · R. Ramakrishnan²

Received: 25 April 2020 / Accepted: 18 November 2020 / Published online: 3 January 2021
© King Fahd University of Petroleum & Minerals 2021

Abstract

EN 10028-P355 GH steel is normalized steel used in high-temperature applications including pipes carrying hot fluids. Fusion welding of such class of steels produces a larger heat affected zone, unwanted metallurgical changes and increased hardness in the weld area. The study explores the possibility of using a solid-state welding process (continuous drive friction welding) on EN 10028-P355 GH steel. The experimentation involves an L_{27} orthogonal array with the welding parameters like frictional pressure, forging pressure, friction time, forging time and rotational speed varied in three levels. The quality characteristics observed include the yield strength, tensile strength, axial shortening and impact toughness. The merits of gray theory are combined the statistical analysing capabilities of response surface methodology in an integrated approach of gray incidence reinforced response surface methodology to select the optimal friction welding inputs (frictional pressure-93.94 MPa, friction time-5.22 s, upset pressure-138.14 MPa, forging time-3.58 s and rotational speed-1282.67 rpm). The optimal friction welding inputs were validated with proper experiments, and microscopic images concerned with optimal bond is also analyzed. The study will offer the guiding database to weld EN 10028-P355 GH steel in solid-state using continuous drive friction welding.

Keywords EN 10028 GH steel · Continuous drive friction welding · Response surface methodology · gray theory · L_{27} orthogonal array

1 Introduction

The EN 10028-P355 GH steel finds its widespread applications in pressure vessels and boilers. The high tensile strength and impact toughness of EN 10028-P355 GH steel makes it a primary choice for tubes and pipes transporting hot fluids in heat exchangers. There are concerns in joining EN 10028-P355 GH steel using the conventional liquid state joining processes. The fusion welding techniques are characterized by the presence of a larger heat affected zone

(HAZ) and consequent changes in the metallurgy of parent, producing corrosion at grain boundaries on a microscopic scale. This could affect the mechanical properties of joint, which is significant in applications at elevated temperature and stress. Hence, joining EN 10028-P355 GH steel in a solid-state could open up the possibilities of minimizing such unwanted mechanical and metallurgical changes. The temperature involved in solid-state processing is considerably lesser than the melting point of parent material hence producing a meager or zero HAZ. The continuous drive friction welding is a joining process employed to join tubes and pipes of both ferrous and non-ferrous materials. The process involves the generation of heat by mechanical rubbing (rotation) of one part with the other half of the joint. The desired rotational speed ensures a constant and continuous stirring at the weld interface and the applied upset pressure produces a bond with a certain amount of flash. Further the volume of material close to the weld interface alone is subjected to plastic deformation, restricting the axial shortening of joint. In the preliminary stages of the formation of a bond,

✉ G. Senthilkumar
nss@pit.ac.in

R. Ramakrishnan
ramkinr@yahoo.com

¹ Department of Mechanical Engineering, Sathyabama Institute of Science and Technology, Chennai, India

² Department of Sports Technology, Tamilnadu Physical Education and Sports University, Chennai, India



the end of the rotating part was made tapered and inserted into a bore ring made of a material with good thermal resistance [1]. During the process, the plastic flow of material was observed at the joint interface. The mechanism regulating the plastic flow of material at the weld interface was important for controlling the amount of flash produced. A sound joint with a reasonably lesser flash was always desired to reduce axial shortening [2]. The observations patented by United Launch Alliance, Inc., had described the essential improvements in hardware employed to produce joints in solid-state [3]. A self-reacting pin tool was also proposed to eliminate the difficulties experienced in using a rigid and static tool in friction stir welding.

Friction welding was used to produce dissimilar steel joints with reasonably good strength and ductility compared to that of the parent material. The investigation revealed that the susceptibility of the weld area to failure under uniaxial loading as the weld interface was the weaker zone due to increased microhardness. The friction welding inputs including frictional pressure, upset pressure, burn off length and rotational speed were found to significantly influence the mechanical properties of joints [4, 5]. The design parameters in friction welding were varied to study their roles in the strength related aspects. The mechanical tests on joints had revealed a higher hardness in the plastic weld zone, while the microhardness variation was found to be lesser in the parent material [6, 7]. In the joints formed between AISI 4140 and AISI 1050 steels, the temperature rise was observed to play a vital role in affecting the quality characteristics of the bonds. The initial rise in temperature was found to be larger, followed by a steady rise with the continuous rotation, and the joints were formed with zero blank spaces [8]. Austenitic stainless steels known for weldability and corrosion resistance were produced with desirable mechanical properties friction welded at high temperatures [9]. Non-ferrous alloys could also be joined by friction welding and proper selection of process parameters could yield a joint efficiency of 89% in as-welded condition [10]. However, the dissimilar joints formed between aluminum and copper showed poor strength as a result of the accumulation of alloying elements and intermetallic compounds at the weld interface [11].

Generally, the friction welded interface included three different regions: unaffected zone, partially deformed zone and fully deformed recrystallized zone. Most of the microstructural changes were observed in the fully deformed and partially deformed zones [12]. A near-perfect bonding strength, close to that of parent material was possible by selecting proper values of friction time and rotational speed. The temperature distribution in the friction interface was mainly dependent on the welding parameters [13]. High strength nickel alloys joined using friction welding displayed a harder and stronger weld zone due to the formation of precipitates [14]. Dissimilar bonds involving maraging steel

and low alloy steel were also formed using continuous drive friction welding. An interlayer of nickel was used as a diffusion barrier to improve the joint strength. The bonds were observed to respond to solutionizing and aging positively during post-weld heat treatment [15]. The tensile strength of steel joints increases with frictional pressure and friction time up to a certain level, but tend to decrease at higher values of these welding inputs. A similar trend was observed with the fatigue strength of joints [16]. Rotational speed and frictional pressure were found to influence the distribution of temperature and plastic flow of material at the weld interface. Optimal values of these welding inputs were observed to produce defect-free joints [17]. Hence, it is observed from the literature that superior quality characteristics of a joint depends primarily on the optimal selection of friction welding parameters like frictional pressure, friction time, upset pressure, forging time, burn off length and rotational speed.

Identifying the proper levels of various friction welding inputs could result in a joint with better quality characteristics. Hence, finding the optimal levels of design variables, their relationships with the responses and understanding the interaction among them is essential to form good joints. Design of experiment and evolutionary algorithms could be used to develop a mathematical relationship between the welding parameters and quality characteristics of the joint. The available literature had revealed a considerable interest in the application of response surface methodology (RSM) and artificial neural network to predict the responses. Optimization could be performed by using simulated annealing, genetic algorithm and particle swarm techniques. Among the three methods, genetic algorithm was observed to outperform the other methods [18]. Genetic algorithm was a good tool for experimental welding optimization even without a model for the process, however, difficulty was experienced in setting its parameters such as population size and number of generations for sufficient sweeping of search space. The technique of RSM technique was found to arrive at a better compromise between the evaluated responses though it struggles in the irregular experimental region [19]. The RSM technique was applied to find the optimal condition of friction welding parameters for joining dissimilar metals D3 tool steel and 304 austenitic stainless steel. The experimentation was based on Box–Behnken design to obtain the highest tensile strength [20]. The process parameters of friction welding were optimized using RSM for joining duplex stainless steel (DSS) UNS S32205. The central composite design (CCD) was used for experimentation. The upset pressure, friction pressure and speed of rotation were identified as most influencing parameters in maximizing the hardness and tensile strength [21, 22].

The application of hybrid techniques was employed for the optimization of process parameters and modeling the response values of various process. These integrated

approaches have opened up the possibilities of combining the merits of the algorithms. The gray relational analysis was coupled with RSM technique for optimization and modeling of responses [22, 23]. The gray Taguchi-RSM was used for optimizing the friction welding parameters to join Al6061/SiC/Al₂O₃ metal matrix Composite [24]. It is a statistical tool used for optimization, and the technique is used to generate response surfaces to study the interaction effects of various design variables. Generally, Box–Behnken design and central composite design are used as the major response surface designs [23, 25, 26]. In a traditional RSM generating a quadratic response surface model for each of the responses, central composite design (CCD) or Box–Behnken design (BBD) is used for experimentation. This limits the study to the effects of design variables on single responses hence restricting the observations concerned with simultaneous optimization [27].

A considerable amount of literature is available in friction welding of similar and dissimilar materials of equivalent grade materials. An equivalent grade material, nuclear grade austenitic stainless steel 321 was joined by using a conventional TIG welding process, and their parameters were optimized using gray relational analysis to improve the mechanical properties of weld joints [28]. The effect of the heat input on the bead width and depth of penetration with various arc lengths was analyzed. The tensile strength measured at weld line (624 MPa) was observed higher than that of base metal (621 MPa). The flux activated—TIG welding process was employed for joining a square-groove butt weld joint of modified 9Cr–1Mo steel and the influence of MnO₂ flux activation on mechanical and metallurgical properties was analyzed. The activated TIG welding improved the depth of penetration and depth-to-width ratio (D/W) compared to the TIG welding process [29]. The Fe–2.25Cr–1Mo steel tube was joined with carbon steel tube using TIG welding process with the application of chromium containing filler material. The formation of Cr₂O₃ due to chromium content improved the corrosion resistance behavior of the weld [30]. The literature related to solid-state joining of EN

10028-P355 GH steel are not enough even the material has major applications in heat exchanger tubes. Further, little attention is observed in welding parameter design involving EN 10028-P355 GH steel within the scientific literature. Hence, the work explores the possibility of forming good quality welded joints using continuous drive friction welding with the objective of offering the guidelines and welding database for joining EN 10028-P355 GH steel using friction welding process. Though applications of RSM with central composite design are available in manufacturing processes, orthogonal arrays-based RSM is limited in the literature. Hence, the scope for simultaneous optimization of multiple responses is widened in the proposed work by application of an integrated approach of gray incidence reinforced response surface methodology for optimal parameter design.

2 Material and Experimental Procedure

2.1 Machine and Material

The EN 10028-P355 GH steel used as heat exchanger tubes is procured in the form of a normalized steel rod of diameter 16 mm. The chemical composition of parent material is as follows: Mn-1.10%, C-0.18%, Si-0.50%, Cr-0.30%, Mo-0.08%, Ni-0.5%, V-0.10, Cu-0.30%, S-0.01% and Fe-remaining. The rods machined to lengths of 130 mm each are subjected to friction welding in a continuous drive friction welding machine (Model: FW-6T) manufactured by RV machine tools, Coimbatore, India. The machine houses a hydraulic chuck with a spindle driven at a maximum speed of 3000 rpm and rated at 12 kW. The servomotor gearbox is used for slide drive, and the friction welding parameters are precisely set by ‘Indra Control VCP-02’ at the operator terminal. The machine has an inbuilt unit of the ‘Rexroth controller’ manufactured by the automation assembly unit of Bosch Rexroth, Germany (Fig. 1a, b).

Figure 1 a Friction welding machine, b operator terminal



Figure 2 a Application of frictional pressure in the initial phase, b upset and formation of flash.

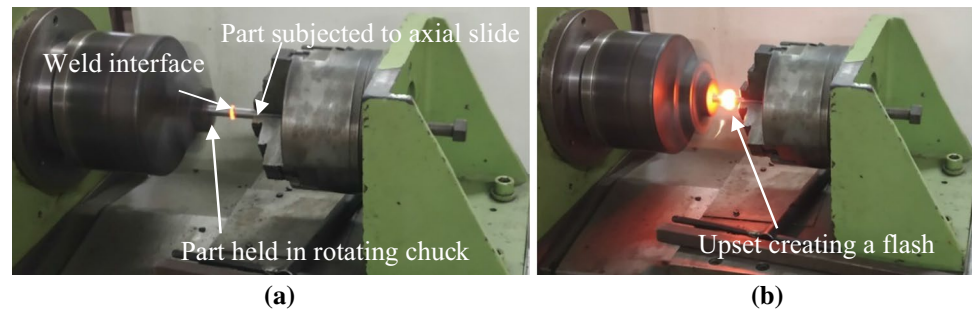


Table 1 Levels of various friction welding inputs

Friction welding inputs	Symbol	Unit	Levels of parameters		
			Level 1	Level 2	Level 3
Frictional pressure	A	MPa	70	90	110
Upset pressure	B	MPa	100	120	140
Frictional time	C	s	3	5	7
Forging time	D	s	3	5	7
Rotational speed	E	rpm	1000	1200	1400

2.2 Experimentation

During friction welding, one half of the joint was attached to spindle drive, precisely controlled by Rexroth while the other half is held stationary and impending to slide. The two parts are allowed to get in contact after ensuring equal overhang on both the parts to be joined. With the required setting of parameters, a smooth transition is ensured across different phases of the formation of joint. Figure 2a, b shows the initial phase, upset and formation of flash at weld interface during the process of friction welding. The predominant welding parameters used in experimentation include the frictional pressure, friction time, upset pressure, forging time and rotational speed [20, 21]. These parameters affect the temperature, and hence, the plastic flow at weld interfaces determining the joint characteristics [4, 6, 8, 16, 22]. The levels of various parameters were found out using the preliminary experimental trials resulting in bonds without any defects/failure on visual inspection. Trials for determining the range of various parameters were conducted based on pre guidance from scientific literature. Table 1 displays the levels of various welding parameters used in experimentation.

Taguchi's orthogonal array (L_{27}) was used to conduct the experiments, which opens the possibility of studying the necessary interaction effects among various design variables [27]. The quality characteristics include the yield strength (YS), ultimate tensile strength (UTS), axial shortening (AS) and impact toughness (IT). To reduce the effects of uncontrollable factors, the trials were conducted



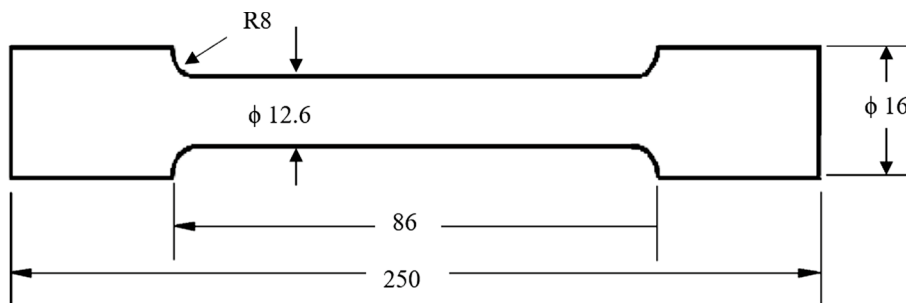
Fig. 3 Sample joints formed during friction welding

at random [20] with necessary replications, and the formed joints were observed for the quality characteristics. The sample joints formed during experimentation are shown in Fig. 3.

The tension test was performed in Instron-Computerized tension tester after preparing the specimen as per the ASTM E8 standard. The layout of specimen for tensile testing is shown in Fig. 4. A few samples of tensile specimen before and after testing are shown in Fig. 5. Failure was observed near the weld interface in most of the samples subjected to tension tests.

Axial shortening was measured as the decrease in length of the final joint obtained at the end of the friction welding process. Impact toughness was primarily studied to observe the effect of larger deformation speeds on the material. The amount of energy absorbed by the specimen during fracture, as observed from the impact test gives a toughness measure of samples. This offers the scope for further studies related to the ductile–brittle transition. Charpy V-notch testing (pendulum type) is performed to find the energy absorbed by samples on dynamic loading as per ASTM E23 standard. The layout of specimen for impact testing is shown in Fig. 6. The sample specimen for the Charpy V-notch test after failure is shown in Fig. 7. The quality characteristics observed in various friction

Fig. 4 Layout of specimen for tensile testing



All the dimensions are in mm

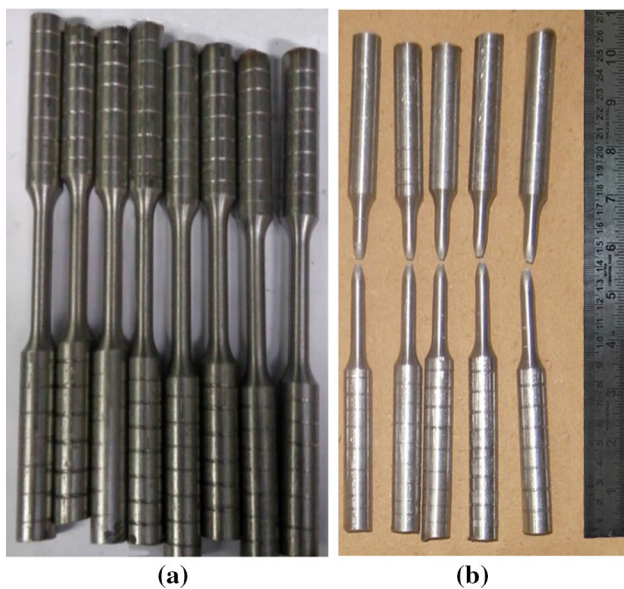
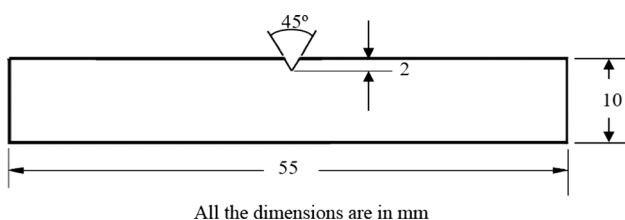


Fig. 5 Samples **a** before tension test, **b** after tension test



All the dimensions are in mm

Fig. 6 Layout of specimen for Charpy V-notch test



Fig. 7 Specimen subjected to Charpy V-notch test

welded joints formed using different combinations of welding inputs (L_{27} orthogonal array) is shown in Table 2.

3 gray Incidence Reinforced Response Surface Methodology

RSM is a statistical approach with a module for modeling the design variables and desirability analysis for optimizing the responses. The effects of parameters on responses are illustrated by 3D surface graphs. The integrated strategy of gray incidence reinforced response surface methodology combines the uncertainty handling ability of gray incidence analysis with the modeling abilities of RSM. The multiple responses observed via experimentations are transformed into a single measure of quality as gray relational grade (GRG). It is used for further modeling using RSM and simultaneous optimization of the welding inputs (design variables). The various steps in gray incidence reinforced response surface methodology are presented in two stages.

3.1 Part I: gray Incidence Analysis

During the first stage of gray incidence, the experimental data are processed by calculating the reciprocal of coefficient of variation termed as the ‘signal-to-noise’ (S/N) ratio. The normalized S/N ratio converts experimental data in the range of zero to one. The processed data are further analyzed by forming gray relational grade and projecting it as the single representative of various outputs obtained from experimentations. The various steps are discussed below.

Step 1 Estimate the S/N ratio (η_{ij}) for each output using the appropriate equation based on its quality characteristics. The three formats in which an output are analyzed include the following: *nominal-the-best*, *smaller-the-better* or *larger-the-better*. A *nominal-the-best* characteristic has a user-defined target value. The target of *smaller-the-better* characteristic is attaining a minimum value of response (zero), while a *larger-the-better* characteristic has a target of infinity i.e. attaining a

Table 2 Levels of various friction welding inputs and observed responses

Trial order	Friction welding inputs					Responses								
	Actual	Random	A	B	C	D	E	YS (MPa)	UTS (MPa)	AS (mm)	IT (J)			
1	7	70	100	3	3	1000	281.95	282.55	483.02	485.10	10.50	10.67	14	15
2	23	70	100	5	5	1200	304.35	304.75	501.60	503.60	16.80	16.63	18	18
3	3	70	100	7	7	1400	314.46	314.06	551.55	553.55	21.10	22.93	21	20
4	4	70	120	3	5	1400	286.54	287.14	525.70	525.70	15.80	15.97	17	17
5	17	70	120	5	7	1000	276.13	275.73	548.55	548.55	22.70	22.70	18	16
6	22	70	120	7	3	1200	290.82	291.54	563.35	562.35	16.20	16.37	19	19
7	2	70	140	3	7	1200	305.39	305.79	592.80	593.80	22.20	22.37	19	18
8	8	70	140	5	3	1400	300.24	300.24	542.80	540.80	20.90	21.07	21	22
9	12	70	140	7	5	1000	310.48	310.88	578.05	576.05	24.80	24.80	20	20
10	14	90	100	3	3	1000	308.25	307.85	584.25	585.25	12.60	12.27	17	18
11	27	90	100	5	5	1200	316.24	316.24	587.10	588.10	17.80	17.80	19	20
12	9	90	100	7	7	1400	320.15	319.55	599.45	600.45	23.60	23.77	22	21
13	25	90	120	3	5	1400	319.51	319.11	581.68	582.95	20.90	20.90	20	20
14	26	90	120	5	7	1000	320.27	320.67	575.70	576.70	21.40	21.07	19	18
15	13	90	120	7	3	1200	313.54	313.74	586.15	589.15	22.40	22.23	20	20
16	16	90	140	3	7	1200	317.87	317.47	584.25	586.25	23.20	23.20	21	22
17	20	90	140	5	3	1400	319.26	319.26	570.10	570.10	20.40	20.40	22	22
18	15	90	140	7	5	1000	319.77	319.97	548.55	547.55	22.10	22.77	20	21
19	5	110	100	3	3	1000	304.14	303.94	549.10	551.10	15.70	15.37	17	17
20	10	110	100	5	5	1200	319.27	319.87	581.40	582.40	21.90	21.23	18	20
21	18	110	100	7	7	1400	330.65	330.85	602.15	601.23	24.60	25.37	21	18
22	6	110	120	3	5	1400	321.54	321.14	600.40	598.40	22.80	22.37	19	18
23	1	110	120	5	7	1000	308.47	309.07	557.55	559.55	21.60	21.27	17	17
24	11	110	120	7	3	1200	319.67	319.67	606.10	605.10	22.70	22.03	18	18
25	24	110	140	3	7	1200	309.82	309.82	593.95	596.95	20.90	21.07	20	18
26	21	110	140	5	3	1400	312.52	311.92	605.15	606.15	25.70	25.87	22	20
27	19	110	140	7	5	1000	310.84	310.44	578.40	579.40	24.20	24.37	20	22

maximum value of output. The S/N ratio (η_{ij}) for such characteristics is calculated by using Eqs. (1) and (2).

$$\text{Smaller-the-better characteristic: } S/N \text{ Ratio}(\eta) = -10 \log_{10} \left(\frac{1}{r} \cdot \sum_{i=1}^r y_{ij}^2 \right) \tag{1}$$

$$\text{Larger-the-better characteristic : } S/N \text{ Ratio}(\eta) = -10 \log_{10} \left(\frac{1}{r} \right) \sum_{i=1}^r \frac{1}{y_{ij}^2} \tag{2}$$

where y_{ij} = observed response values, $i = 1, 2, 3 \dots r$, and $j = 1, 2, \dots m$, r = number of replications, m = number of observations.

Step 2 Estimate the normalized S/N ratio (Z_{ij}) using Eq. (3) to reduce the variability among the calculated values of S/N ratio for various responses. ‘ n ’ represents the number of trials.

$$Z_{ij} = \frac{y_{ij} - \min(y_{ij}, i = 1, 2, \dots, n)}{\max(y_{ij}, i = 1, 2, \dots, n) - \min(y_{ij}, i = 1, 2, \dots, n)} \tag{3}$$

Step 3 calculate the gray incidence coefficient (γ) from the normalized S/N ratio values using Eq. (4)

$$\gamma_i^j = \frac{\Delta \min + \xi \Delta \max}{\Delta_{oj}(i) + \xi \Delta \max} \tag{4}$$

where $i = 1, 2, \dots, n$ and $j = 1, 2, \dots, m$, n is the number of responses and m is the number of trials.

$\Delta_{oj} = \left\| z_o(i) - z_j(i) \right\|$, $z_o(i)$ is the reference sequence ($z_o(i) = 1; i = 1, 2, \dots, n$) and $z_j(i)$ is the specific comparison sequence.

$\Delta \min = \min_{\forall j \in i} \min_{\forall i} \left\| z_o(i) - z_j(i) \right\|$ is the smallest value of $z_j(i)$, $\Delta \max = \max_{\forall j \in i} \max_{\forall i} \left\| z_o(i) - z_j(i) \right\|$ is the largest value of $z_j(i)$, and ‘ ξ ’ is the distinguishing coefficient whose value is taken as 0.25.

Step 4 Find the GRG values (γ_i) for every trial using Eq. (5)

$$GRG_i = \frac{1}{n} \sum_{i=1}^n (\gamma_i). \tag{5}$$

3.2 Part II: GRG Reinforced RSM

The GRG value for various trials is seen as a single quality measure representing various responses. The GRG value for various experimental conditions is used in the RSM technique as a single response and a polynomial model for GRG value is generated. The response surfaces plots are also generated to observe the influence of welding inputs.

Step 5 Execute the analysis of variance (ANOVA) using GRG values to find the significant contribution of welding inputs.

Step 6 Develop a quadratic model to relate the GRG with various inputs and their interactions. Test the model fitness with the experimental data.

Step 7 Plot the response surfaces (3D) graphs to study the effects of various welding inputs on GRG and use desirability analysis to find the optimal welding condition. Validate the same via experimentations.

4 Results and Discussion

4.1 gray Incidence Analysis and GRG Values

gray incidence analysis was performed using the gray theory which uses S/N ratio as the preliminary index and gives solutions that are more appropriate to real-world problems [20]. The three quality characteristics studied via experimentations (YS, UTS and IT) were treated as ‘larger-the-better’ characteristics with an intended magnitude of one, while the fourth response (AS) was analyzed as the ‘smaller-the-better’ characteristic with a desired value of zero. The calculated S/N values of various responses were subjected to linear normalization to align those towards normal distribution and make the values of design variables more comparable. The normalized values of S/N ratios are presented in Table 3. The GRG values were obtained using the GRC

values calculated using Eq. (6). The GRG functions as a representative for the various measured responses, deserving a higher value regardless of their nature. The variations in GRG values for the 27 experimental trials are described graphically in Fig. 8. The maximum observed value of GRG was 0.6370 (21st trial), indicating a closer proximity of the experimental conditions to a near-optimal one.

4.2 Second-Order Polynomial for GRG (Fitness and Adequacy)

The methodology of RSM uses a mathematical technique for model building. The design variables used in friction welding were mapped with the quality characteristics observed in solid-state joints in terms of GRG. A quadratic model [Eqs. (6), (7)] which was a polynomial of order two was formed to relate the various welding inputs with GRG using Design-Expert software. The formulated model includes both individual and interaction effects of various welding inputs on GRG thus offering the scope to observe the mathematical behavior within the system. Equations (6, 7) represent the representative of responses (GRG) in terms of coded and actual factors respectively. The insignificant terms were excluded (model reduction) to make it less expensive computationally, but preserving the closeness and stability of actual model [20]. A considerable reduction in the number of experimental trials was realized with the L_{27} orthogonal array compared to the conventional experimental designs (CCD/BBD) used with RSM [27].

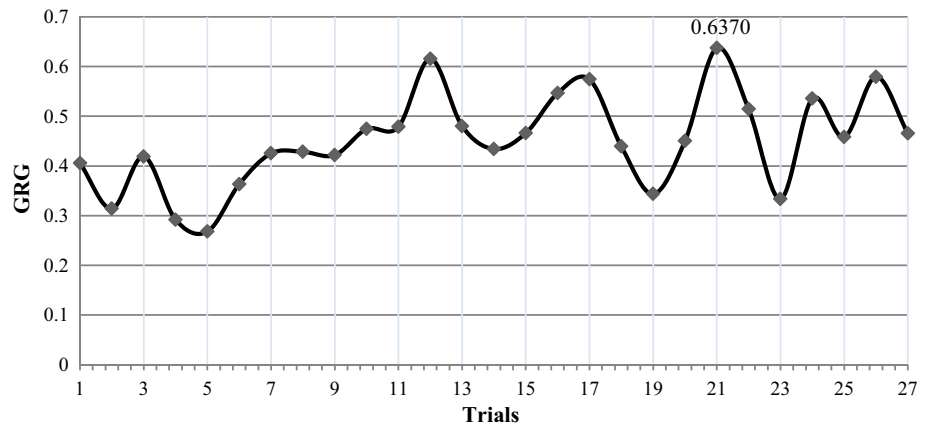
$$\begin{aligned} GRG = & +0.50 + 0.054 \times A + 0.057 \times B + 0.064 \\ & \times C - 0.043 \times D + 0.052 \times E + 0.020 \\ & \times A \times C + 0.045 \times A \times E - 0.082 \times B \times C \\ & + 0.080 \times B \times D + 0.091 \times C \times D - 0.076 \times A^2 \end{aligned}$$

$$\begin{aligned} GRG = & +0.014862 + 0.020672 \times A + 3.03400 \times 10^{-3} \\ & \times B + 0.11713 \times C - 0.37594 \times D - 7.58611 \times 10^{-4} \\ & \times E + 5.01554 \times 10^{-4} \times A \times C + 1.13312 \times 10^{-5} \\ & \times A \times E - 2.04031 \times 10^{-3} \times B \times C + 2.00232 \times 10^{-3} \\ & \times B \times D + 0.022870 \times C \times D - 1.89203 \times 10^{-4} \times A^2 \end{aligned}$$

Analysis of variance (Table 4) was carried out to study the model adequacy and fitness in relating the welding inputs with GRG [23, 24]. This could help in understanding the importance of model coefficients identified using Design-Expert software in forming a technical link with responses represented by GRG. The polynomial model was found to be significant with an F value of 14.97 and a p value of less than 0.0001, declaring the minimal effects of noise factors. The p value probability less than 0.05 indicates the substantial importance of all the terms in the model including frictional pressure (A), upset pressure (B), friction time

Table 3 Calculations leading to the performance index

Trial	S/N ratio				Normalized S/N ratio				gray relational co-efficient (GRC)				GRG
	YS	UTS	AS	IT	YS	UTS	AS	IT	YS	UTS	AS	IT	
1	49.013	53.697	-20.493	23.212	0.125	0.000	1.000	0.000	0.222	0.200	1.000	0.200	0.4055
2	49.673	54.024	-24.463	25.105	0.545	0.168	0.487	0.521	0.354	0.231	0.327	0.343	0.3139
3	49.946	54.847	-26.863	26.227	0.718	0.591	0.176	0.829	0.470	0.379	0.233	0.594	0.4189
4	49.153	54.415	-24.019	24.609	0.214	0.369	0.544	0.384	0.241	0.284	0.354	0.289	0.2919
5	48.816	54.784	-27.121	24.564	0.000	0.558	0.143	0.372	0.200	0.361	0.226	0.285	0.2679
6	49.283	55.008	-24.235	25.575	0.297	0.673	0.516	0.650	0.262	0.433	0.341	0.417	0.3632
7	49.703	55.465	-26.960	25.334	0.563	0.908	0.164	0.584	0.364	0.731	0.230	0.375	0.4251
8	49.549	54.677	-26.438	26.642	0.466	0.503	0.231	0.943	0.319	0.335	0.245	0.815	0.4284
9	49.846	55.224	-27.889	26.021	0.655	0.784	0.044	0.772	0.420	0.537	0.207	0.523	0.4218
10	49.772	55.339	-21.893	24.850	0.608	0.843	0.819	0.450	0.389	0.615	0.580	0.313	0.4741
11	50.000	55.382	-25.008	25.792	0.752	0.865	0.416	0.710	0.502	0.649	0.300	0.463	0.4785
12	50.099	55.562	-27.489	26.642	0.815	0.958	0.095	0.943	0.575	0.856	0.217	0.815	0.6154
13	50.084	55.303	-26.403	26.021	0.806	0.825	0.236	0.772	0.563	0.588	0.247	0.523	0.4801
14	50.116	55.211	-26.541	25.334	0.826	0.778	0.218	0.584	0.589	0.529	0.242	0.375	0.4339
15	49.929	55.382	-26.973	26.021	0.707	0.865	0.162	0.772	0.460	0.650	0.230	0.523	0.4658
16	50.040	55.347	-27.310	26.642	0.777	0.847	0.119	0.943	0.529	0.621	0.221	0.815	0.5463
17	50.083	55.119	-26.193	26.848	0.805	0.730	0.263	1.000	0.562	0.481	0.253	1.000	0.5739
18	50.099	54.776	-27.019	26.227	0.815	0.554	0.156	0.829	0.575	0.359	0.229	0.594	0.4393
19	49.659	54.809	-23.826	24.609	0.535	0.571	0.569	0.384	0.350	0.368	0.367	0.289	0.3434
20	50.091	55.297	-26.677	25.539	0.810	0.822	0.200	0.640	0.568	0.584	0.238	0.410	0.4501
21	50.390	55.587	-27.954	25.724	1.000	0.971	0.035	0.691	1.000	0.895	0.206	0.447	0.6370
22	50.139	55.554	-27.076	25.334	0.841	0.954	0.149	0.584	0.611	0.844	0.227	0.375	0.5141
23	49.793	54.941	-26.622	24.609	0.621	0.639	0.207	0.384	0.397	0.409	0.240	0.289	0.3337
24	50.094	55.644	-26.993	25.105	0.812	1.000	0.160	0.521	0.571	0.999	0.229	0.343	0.5353
25	49.822	55.497	-26.438	25.539	0.639	0.924	0.231	0.640	0.409	0.767	0.245	0.410	0.4579
26	49.889	55.644	-28.227	26.415	0.682	1.000	0.000	0.881	0.440	1.000	0.200	0.677	0.5792
27	49.845	55.252	-27.706	26.415	0.654	0.799	0.067	0.881	0.419	0.554	0.211	0.677	0.4653

Fig. 8 Plot of GRG values for different experimental trials

(C), forging time (D), rotational speed (E) and their interactions (AE, BC, BD and CD). Second-order of term A (frictional pressure) was also found to be significant in influencing the GRG and hence the responses. The quadratic model

was capable of simulating the solid-state friction welding conditions in EN 10028-P355 steel.

The *R*-squared value (coefficient of determination) and adequate precision value is shown in Table 5. The *R*-squared value is a statistical measure to understand the closeness

Table 4 ANOVA for response surface quadratic model

Source	Sum of squares	Degrees of freedom	Mean sum of square	F value	p value	Remarks
Model	0.212782	11	0.019344	14.97374	<0.0001	Significant
A—Frictional pressure	0.053276	1	0.053276	41.23997	<0.0001	
B—Upset pressure	0.025479	1	0.025479	19.723	0.0005	
C—Friction time	0.020368	1	0.020368	15.76649	0.0012	
D—Forging time	0.009158	1	0.009158	7.089374	0.0177	
E—Rotational speed	0.007017	1	0.007017	5.431853	0.0341	
AC	0.00483	1	0.00483	3.73874	0.0723	
AE	0.024652	1	0.024652	19.08267	0.0006	
BC	0.011656	1	0.011656	9.0228	0.0089	
BD	0.011226	1	0.011226	8.689914	0.0100	
CD	0.029291	1	0.029291	22.67372	0.0003	
A ²	0.034366	1	0.034366	26.60214	0.0001	
Residual	0.019378	15	0.001292			
Cor total	0.232159	26				

Table 5 Coefficient of determination and model discrimination

SD	0.036	R-squared	0.9378
Mean	0.45	Adj R-squared	0.8553
C.V. %	7.98	Pred R-squared	0.7114
PRESS	0.067	Adeq precision	14.205

of data to the regression line. A higher value of the coefficient of determination (greater than 0.7) is desired to ensure better fitness of the generated model to experimental data. The R-squared value of 0.9378, nearer to unity ensures a good fit between the generated polynomial equation and data measured within the welding domain. Though the predicted R-squared value (0.7114) was observed to be lesser than the adjusted R-squared value (0.8553), it proves the capability of the model to predict the response for a new set of observations in welding inputs. The predicted R-squared value (0.7114) observed from Table 5 was reasonable in preventing an overfit model, which would explain noise otherwise. Adequate precision could compare the range of predictions from the polynomial model to the associated errors. Adequate Precision was observed to be 14.205 (a value greater than 4 is desired), which proves the sufficiency in model discrimination in terms of signal adequacy. Hence the generated polynomial equation can be deemed fit and adequate in describing the relationship between the welding inputs and response represented in terms of GRG.

The closeness of actual and predicted values of response (GRG) for the 27 trials is shown in Fig. 9 (Plot of the predicted versus actual GRG values). The points are closer to the diagonal regression line without a foggy pattern proving the model fitness [24]. The plot of internally studentized

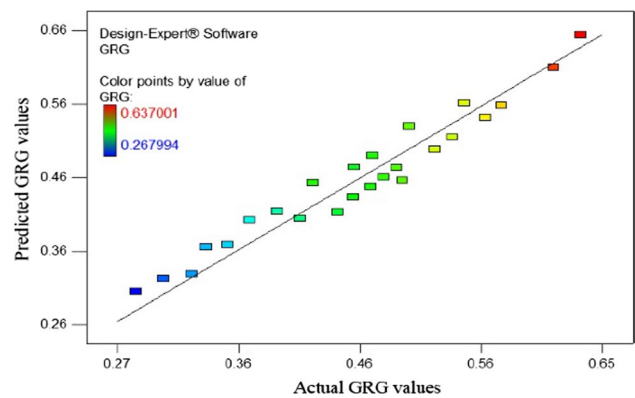


Fig. 9 Scatter plot of predicted versus actual GRG values

residuals is shown in Fig. 10. It considers the difference in predicted and observed values of GRG along with the standard deviation. The majority of the residuals are observed to be positive or along the diagonal line with an almost symmetric distribution without any clear patterns. The randomness in the residual plot further ascertains the fitness of the generated model for the response.

4.3 Analysis of Response Surface Plots

The various welding parameters including the frictional pressure, friction time, upset pressure, forging time and rotational speed, along with their interactions were observed to influence the yield strength, tensile strength, impact toughness and axial shortening significantly. Frictional pressure along with a defined rotational speed helps in creating the required temperature at the weld interface. The heat generation at the

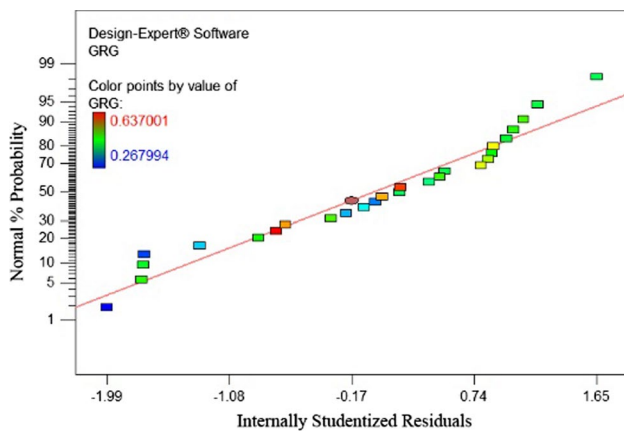


Fig. 10 Plot of studentized residuals to ascertain fitness

localized region is due to the rubbing action of irregularities in the mating surface. The constant frictional pressure ensures flattening of irregularities at the weld interface eliminating surface preparation in friction welding. A moderate value of frictional pressure (93 MPa) was observed to produce a better response as observed from the response surface plots (Fig. 11a, b). However, a moderate level of friction time (5.22 s) was desired to generate the heat and necessary temperature at the interface (Fig. 11b–d). A higher value of upset pressure (138 MPa) was found to produce a larger GRG (Fig. 11c, e) and hence, an improved response. The effect of upset along with the frictional energy input softens the materials assuring a plastic flow at the interface in the form of flash creating a good bond. When the forging pressure was maintained for more time, a considerable axial shortening was observed, and GRG was observed to decrease. Increased forging time allows for more heat dissipation in lesser time by increasing the surface area of flash. This could cause an increased hardness at the weld interface area. Hence, a small forging time was desired as observed from the plots (Fig. 11d, e). Also heat transfer by forced convective mode was realized at higher rotational speeds resulting in temperature drop at an increased rate. Hence, a moderate value of rotational speed (1282 rpm) was observed to be effective in producing better response (Fig. 11a).

4.4 Desirability Analysis on GRG Values and Ramp Graph

The technique of desirability analysis uses a desirability function to identify the scale-free value of desirability for the various responses [27]. The desirability function used in analysis of the calculated GRG values is of ‘larger-the-better’ type which forms the individual values of desirability ranging from zero to one. The combination of friction welding inputs producing the maximum value of desirability

was identified and marked as the near-optimal condition (frictional pressure-93.94 MPa, friction time-5.22 s, upset pressure-138.14 MPa, forging time-3.58 s and rotational speed-1282.67 rpm). The outcome of desirability analysis is presented in Table 6. The ramp graph with optimal levels of welding inputs is shown in Fig. 12. The ramp graphs of individual welding inputs are combined and presented for the greatest overall desirability. The red dot on each ramp shows the most desired level of each welding input within the range chosen for experimental trials, hence representing the highest value of GRG (0.6508).

4.5 Welding Trial Using Predicted Optimal Values of Inputs

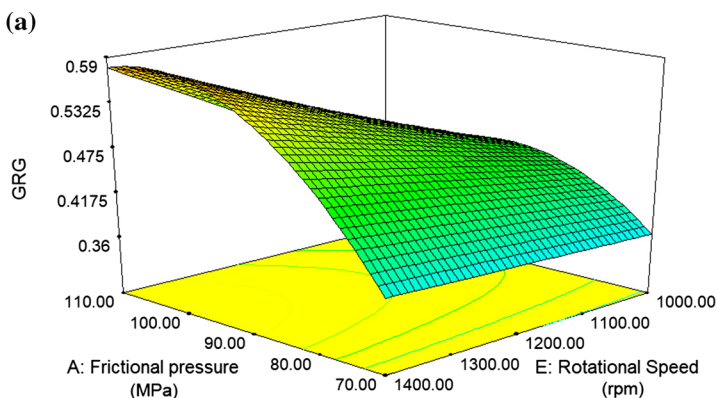
A proper experimental endorsement of near-optimal setting of friction welding inputs (frictional pressure-93.94 MPa, friction time-5.22 s, upset pressure-138.14 MPa, forging time-3.58 s and rotational speed-1282.67 rpm) becomes important to validate the approach of gray incidence reinforced response surface methodology and confirm the improvement in the observed quality characteristics. The outputs of experimental trial (No. 21) with the largest calculated value of GRG (0.6370) were compared with outputs obtained with the optimal setting of welding inputs predicted by gray incidence reinforced response surface methodology. Improvements were observed in the quality characteristics of the joint formed with optimal welding inputs substantiating the approach adopted for multi-response optimization. The properties of joint obtained with optimal parameters are $YS = 339.42$ MPa, $UTS = 612.21$ MPa and $IT = 27$ J, and properties of base metal are $YS = 292$ MPa, $UTS = 528$ MPa, $IT = 23.90$ J. It was observed that the YS and UTS are appeared higher than the values observed at base metal. The improvement in impact toughness appears minimal, but still the value (23.90 J) appears closer to the impact toughness value of parent material (27 J), during Charpy V-notch testing. The axial shortening obtained with the optimal setting of welding inputs was not significantly remarkable (20.75 mm). However, tensile strength and impact toughness were observed to be good at moderate/higher values of axial shortening. Hence, a good bond which promises good mechanical properties can be obtained with only reasonable values of shortening (Table 7).

4.6 Macroscopic and Microscopic Examination of Optimal Joint

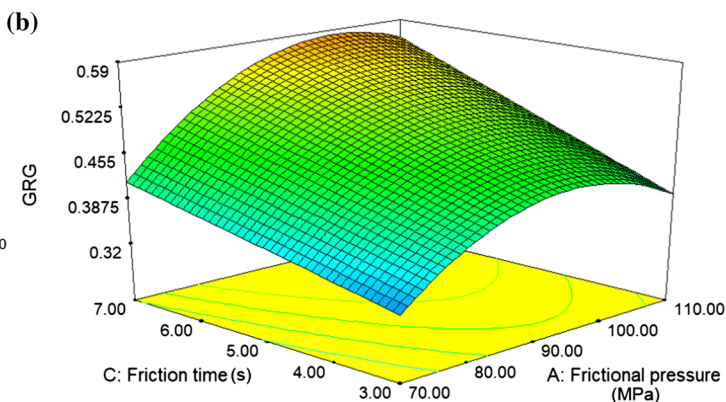
The joint formed with an optimal welding input setting is shown in Fig. 13a, b. The heat flux generated due to frictional pressure and rotational speed creates the necessary thermal input for the softening of material closer to the weld interface. The application of optimal upset pressure creates

Fig. 11 Response surface plots displaying the parameter effects on GRG, **a** frictional pressure and rotational speed, **b** friction time and frictional pressure, **c** friction time and upset pressure, **d** forging time and friction time, **e** upset pressure and forging time

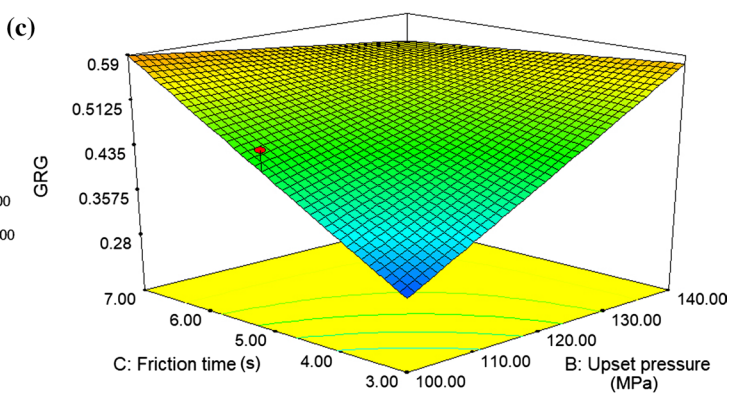
Design-Expert® Software
 GRG
 0.637001
 0.267994
 X1 = A: Frictional pressure
 X2 = E: Rotational Speed
 Actual Factors
 B: Upset pressure = 120.00
 C: Friction time = 5.00
 D: Forging time = 5.00



Design-Expert® Software
 GRG
 0.637001
 0.267994
 X1 = A: Frictional pressure
 X2 = C: Friction time
 Actual Factors
 B: Upset pressure = 120.00
 D: Forging time = 5.00
 E: Rotational Speed = 1200.00



Design-Expert® Software
 GRG
 0.637001
 0.267994
 X1 = B: Upset pressure
 X2 = C: Friction time
 Actual Factors
 A: Frictional pressure = 90.00
 D: Forging time = 5.00
 E: Rotational Speed = 1200.00



Design-Expert® Software
 GRG
 0.637001
 0.267994
 X1 = C: Friction time
 X2 = D: Forging time
 Actual Factors
 A: Frictional pressure = 90.00
 B: Upset pressure = 120.00
 E: Rotational Speed = 1200.00

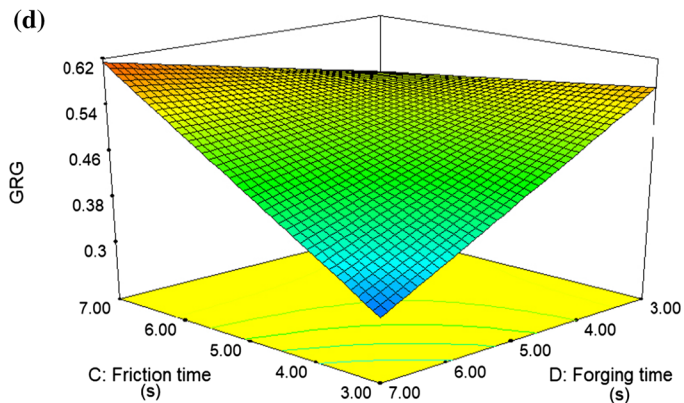


Fig. 11 (continued)

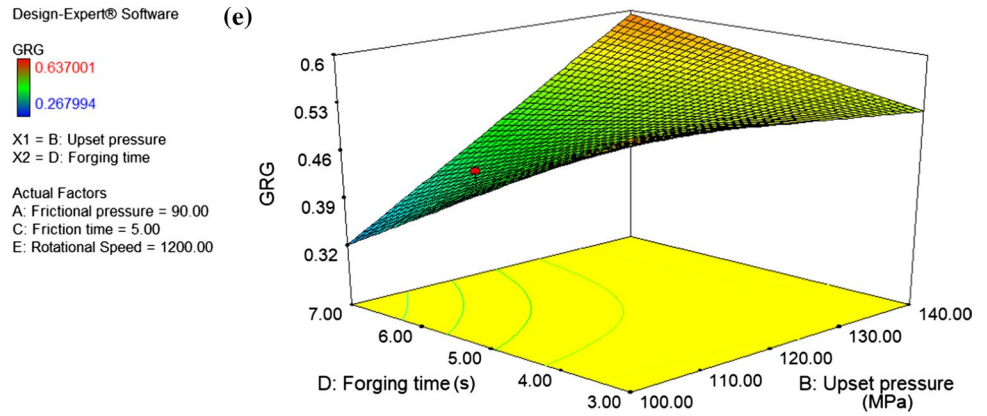


Table 6 Optimal levels of friction welding inputs

Symbol	Welding inputs	Optimal level	Low level	High level
A	Frictional pressure	93.944	70	110
B	Upset pressure	138.147	100	140
C	Frictional time	5.22	3	7
D	Forging time	3.58	3	7
E	Rotational speed	1282.67	1000	1400
Response	Prediction	SE mean	95% CI low	95% CI high
GRG	0.65088	0.06041	0.520419	0.780006

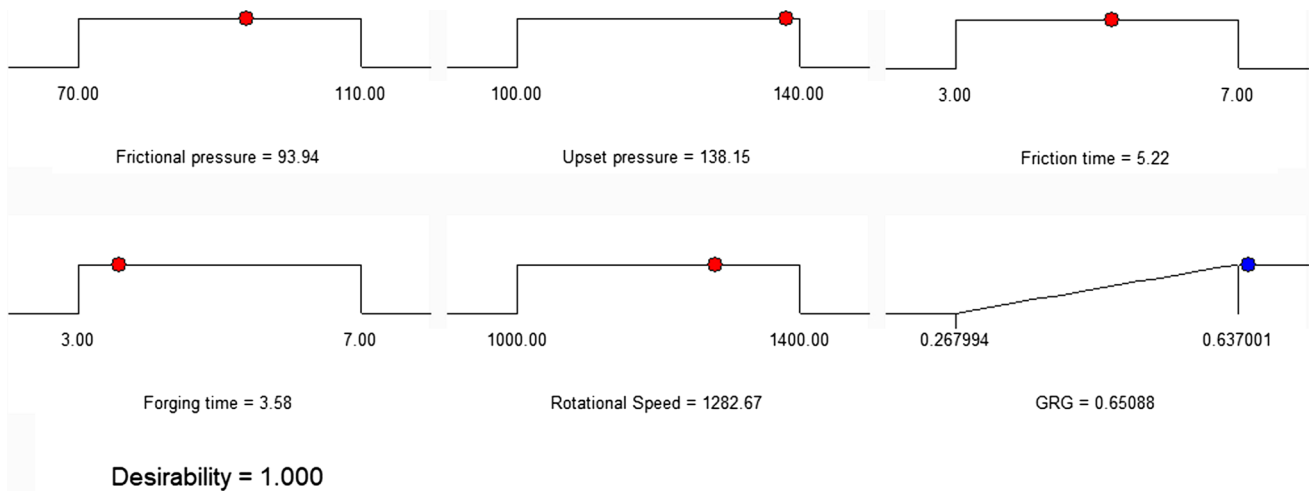


Fig. 12 Ramp graph with optimal level of friction welding inputs

Table 7 Responses obtained with optimal friction welding inputs

Responses	Initial setting	Optimal setting	Enhancement
GRG	0.637	0.65088	0.01388
Yield strength (MPa)	330.62	339.42	8.80
Ultimate tensile strength (MPa)	600.54	612.21	11.67
Axial shortening (mm)	24.15	20.75	3.40
Impact toughness (J)	21.70	23.90	2.20

plastic movement of material closer to interface radially outwards in the form of flash. The curl of parent material in the form of flash was evident, and the weld penetration was thoroughly complete as the weld line was not visible in Fig. 13b. Macroscopic examination further reveals the uniform width of flash, portraying the goodness of bond. The stereo microscope (model SZX16) equipped with DP series digital camera, and an inbuilt imaging software was used to analyse the microstructural characteristics near the weld area (Figs. 14, 15). The weld zone including the interface is seen along with the advancing and receding parts of the joint.

The microstructure of the tensile and impact specimen formed from the bonds with optimal parameter setting is shown in Fig. 14a, b. In both the microstructures, a small amount of pearlitic phase and predominantly ferritic phases are seen. However, pearlite itself is made of ferritic and cementite bonds [6, 8]. The grains appear to be pulled along the direction of uniaxial loading in tensile specimen (Fig. 14a), however, a relatively equi-axed grain is seen in impact specimen (Fig. 14b).

The region circled in Fig. 15a is enlarged to make a clear picture of the different zones near the weld area. Three different regions observed near the weld area

Fig. 13 a Weld interface of optimal joint, b longitudinal cut section revealing flash.

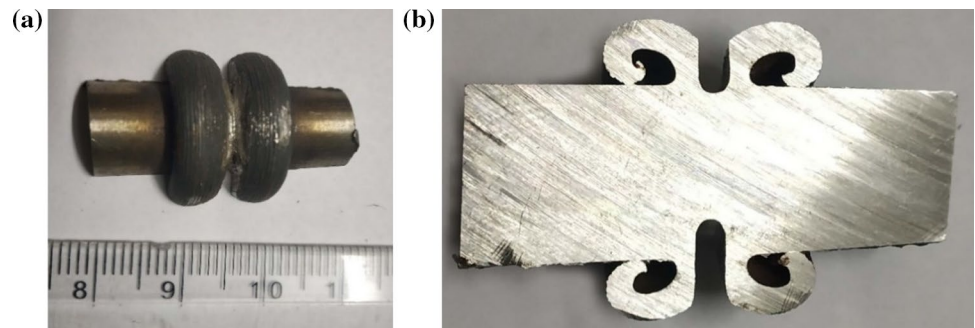


Fig. 14 Microstructure of a tensile specimen, b impact specimen

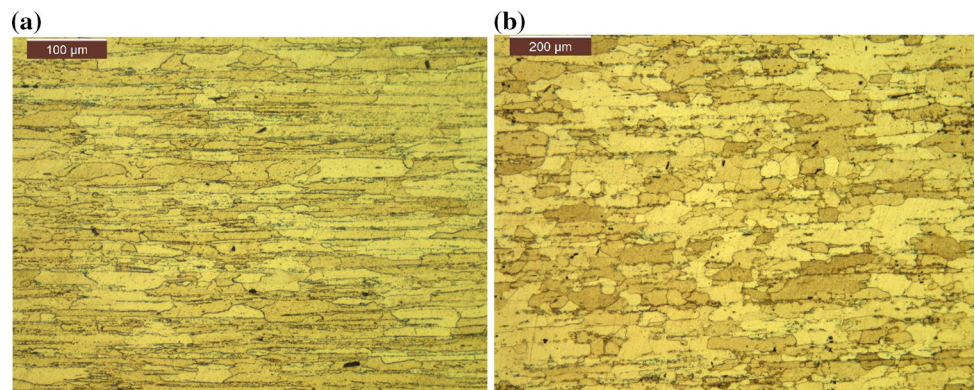
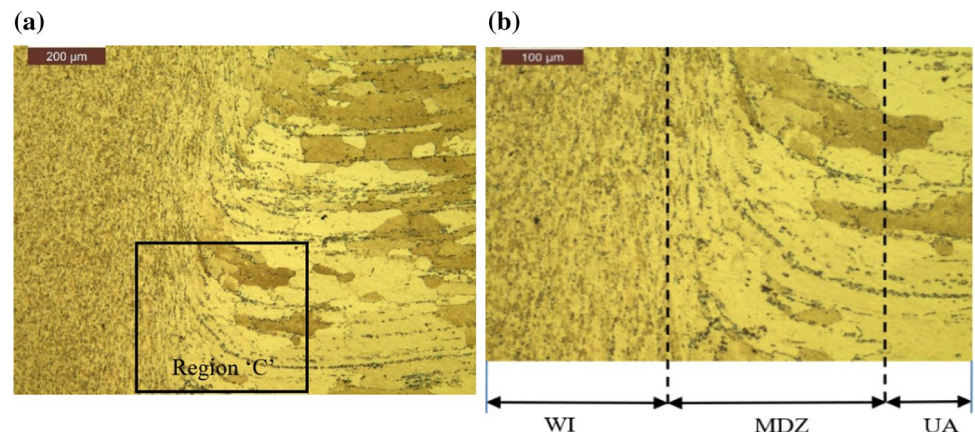


Figure 15 a Weld interface of optimal joint, b different areas near weld line



include the weld interface (WI), moderately deformed area (MDA) and the unaffected area (UA) (Fig. 15 b). The microstructures on the weld interface are characterized by the dynamic recrystallization due to higher rotational speed. The weld interface appears relatively darker compared to the other areas, as it was subjected to high temperature, stress and deformation. The grains appear dragged in the moderately deformed zone because of torque experienced by rotation at higher temperatures. More drag was found in the advancing part of the joint compared to the retreating half. The unaffected area signals the end of plastic flow and the onset of parent material away from the joint interface on both sides. Hence, the softening of material due to thermal input was more evident in the weld interface and moderately deformed zone. The remaining part of parent material was unaffected by temperature and stress hence reducing the chances of undesirable microstructural changes and degradation of properties a possibility in fusion welded joints. The fractured surface of bond subjected to tensile loading is shown in the scanning electron microscope (SEM) images in Fig. 16a–c. Fracture was observed near the weld area as it happened in most of the experimental trials.

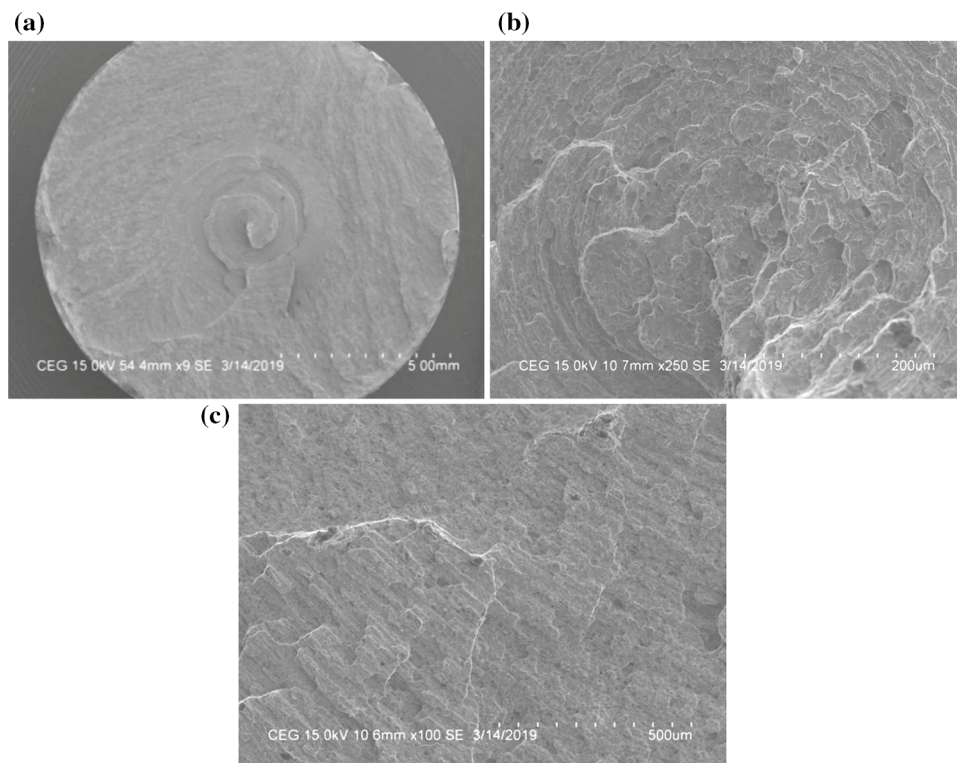
A gross permanent deformation (necked down) was observed near the center of the workpiece in Fig. 16a, and a closer examination reveals the microfractures and smaller voids, which appear after the specimen was

stressed beyond tensile strength (Fig. 16b). The plastic deformation from the necked down area is also visible in Fig. 16c. These are primarily the features or patterns observed in ductile failure in uniaxial tension. The Vicker's hardness values were measured from the weld line towards unaffected parent material on both sides of the weld zone as per the ASTM E-18 standard with the total test force of 100 g for 10 s time. The hardness values measured at the WI, MDA and UA for the optimal joint were 204, 181 and 168 respectively. The joint obtained using initial input parameter setting (Trial No: 21) was found to possess a hardness value of WI, MDA and UA are 198, 178 and 166 respectively. Hence, it was observed that the hardness in the weld zone is relatively higher than that in the unaffected zone of parent material.

5 Conclusion

An effective attempt has been made to joint EN 10028-P355 GH steel in solid-state and possibility of forming good quality welded joints using continuous drive friction welding was also explored. The scope for simultaneous optimization of multiple responses is widened by authorizing an integrated approach of gray incidence reinforced response surface methodology for optimal parameter selection. A notorious reduction in the number of experiments was observed, as L_{27} orthogonal array was used in experimental trials unlike the

Figure 16 a Fractured surface, b voids and coalescence, c closer look at 'necked down' surface



conventional strategies using CCD or BBD with traditional RSM to arrive at the optimal friction welding inputs. The conclusions drawn include the following.

1. The gray incidence reinforced response surface methodology was effective in predicting the near-optimal welding condition (frictional pressure-93.94 MPa, friction time-5.22 s, upset pressure-138.14 MPa, forging time-3.58 s and rotational speed-1282.67 rpm) for joining EN 10028-P355 GH steel in a solid-state.
2. The developed quadratic model was adequate and effective in relating the various welding inputs and predicting the responses in terms of gray relational grade. The predicted and experimentally observed values were found to be reasonably closer demonstrating the model adequacy.
3. In addition to the individual welding parameters, their interactions were also observed to influence the quality characteristics of the joints. A ductile pattern was found in the fractured surface of joint.
4. The optimal welding inputs predicted by the integrated approach of gray incidence reinforced response surface methodology were found to improve the tensile strength and impact toughness. However, a less significant reduction in axial shortening could be better understood from the point of formation of a good bond with reasonably improved strength.

The findings of study could offer the sought-after guidelines for joining EN 10028-P355 GH steel in solid-state using continuous drive friction welding. The generated polynomial equations along with the experimentations will provide the necessary databank for improving the joining characteristics of material employed in boilers and pressure vessels, where the quality of joints is of utmost importance. The results could contribute in enhancing the engineering applications of the material and usage of gray incidence reinforced response surface methodology in different manufacturing strategies. The scope can be extended further to modeling the temperature at the weld interface, correlating the same with joint properties and studying the effects on ductile–brittle transition.

Acknowledgements The authors would wish to extend their sincere gratitude to the facilities and guidance offered by CEMAJOR LAB, Department of Manufacturing Engineering, Annamalai University, Chidambaram, Tamilnadu, India to carry out the investigation.

Compliance with Ethical Standards

Conflict of interest The authors declare no possible conflict of interest regarding the research, authorship and publication of this article.

References

1. Terabayashi, T.: Method of Jointing Pipes by Friction Welding. Patent No. US4331280A (1982)
2. Benn, B.L.; Towler, B.: Control of Friction and Inertia Welding Processes. Patent No. US 4757932A (1988)
3. Potter, D.M.; Hansen, R.K.: Friction Welding Apparatus, System and Method. Patent No. US8123104B1 (2012)
4. Ananthapadmanaban, D.; Seshagiri Rao, V.; Abraham, N.; Prasad Rao, K.: A study of mechanical properties of friction welded mild steel to stainless steel joints. *Mater. Des.* **30**(7), 2642–2646 (2009)
5. Selvamani, S.T.; Vigneshwar, M.; Palanikumar, K.; Jayaperumal, D.: The corrosion behavior of fully deformed zone of friction welded low chromium plain carbon steel joints in optimized condition. *J. Braz. Soc. Mech. Sci. Eng.* **40**, 305–317 (2018)
6. Sathiya, P.; Aravindan, S.; Noorul Haq, A.: Effect of friction welding parameters on mechanical and metallurgical properties of ferritic stainless steel. *Int. J. Adv. Manuf. Technol.* **31**(11–12), 1076–1082 (2007)
7. Ravi Shankar, A.; Suresh Babu, S.; Ashfaq, M.: Dissimilar joining of Zircaloy-4 to Type 304L stainless steel by friction welding process. *J. Mater. Eng. Perform.* **18**, 1272–1279 (2009)
8. Celik, S.; Ersozlu, I.: Investigation of the mechanical properties and microstructure of friction welded joints between AISI 4140 and AISI 1050 steels. *Mater. Des.* **30**(4), 970–976 (2009)
9. Sahin, M.; Cil, E.; Misirli, C.: Characterization of properties in friction welded stainless steel and copper materials. *J. Mater. Eng. Perform.* **22**(3), 840–847 (2012)
10. Rafi, H.K.; Janaki Ram, G.D.; Phanikumar, G.; Prasad Rao, K.: Microstructure and tensile properties of friction welded aluminum alloy AA7075-T6. *Mater. Des.* **31**(5), 2375–2380 (2010)
11. Sahin, M.: Joining of aluminium and copper materials with friction welding. *Int. J. Adv. Manuf. Technol.* **49**(5–8), 527–534 (2010)
12. Ahmad Fauzi, M.N.; Uday, M.B.; Zuhailawati, H.; Ismail, A.B.: Microstructure and mechanical properties of alumina-6061 aluminum alloy joined by friction welding. *Mater. Des.* **31**(2), 670–676 (2010)
13. Luo, J.; Wang, X.; Liu, D.; Li, F.; Xiang, J.: Inertia radial friction welding joint of large size H90 Brass/D60 steel dissimilar metals. *Mater. Manuf. Process.* **27**(9), 930–935 (2012)
14. Huang, Z.W.; Li, H.Y.; Baxter, G.; Bray, S.; Bowen, P.: Electron microscopy characterization of the weld line zones of an inertia friction welded superalloy. *J. Mater. Process. Technol.* **211**(12), 1927–1936 (2011)
15. Madhusudhan Reddy, G.; Venkata Ramana, P.: Role of nickel as an interlayer in dissimilar metal friction welding of maraging steel to low alloy steel. *J. Mater. Process. Technol.* **212**(1), 66–77 (2012)
16. Sahin, M.: Joining with friction welding of high-speed steel and medium carbon steel. *J. Mater. Process. Technol.* **168**(2), 202–210 (2009)
17. Seli, H.; Ismail, A.I.M.; Rachman, E.; Ahmad, Z.A.: Mechanical evaluation and thermal modeling of friction welding of mild steel and aluminium. *J. Mater. Process. Technol.* **210**(9), 1209–1216 (2010)
18. Benyounis, K.Y.; Olabi, A.G.: Optimization of different welding processes using statistical and numerical approaches—a reference guide. *Adv. Eng. Softw.* **39**(6), 483–496 (2008)
19. Correia, D.S.; Goncalves, C.V.; Cunha, S.S.; Ferraresi, V.A.: Comparison between genetic algorithms and response surface methodology in GMAW welding optimization. *J. Mater. Process. Technol.* **160**(1), 70–76 (2005)
20. Haribabu, S.; Cheepu, M.; Devuri, V.; Kantumuchu, V.C.: Optimization of welding parameters for friction welding of 304



- stainless steel to D3Tool steel using response surface methodology. *Technol-Soc.* **1**, 427–437 (2020)
21. Ajith, P.M.; Afsal Husain, T.M.; Sathiya, P.; Aravindan, S.: Multi-objective optimization of continuous drive friction welding process parameters using response surface methodology with intelligent optimization algorithm. *J. Iron Steel Res. Int.* **22**, 954–960 (2015)
 22. Santhanakumar, M.; Adalarasan, R.; Rajmohan, M.: Experimental modeling and analysis in abrasive waterjet cutting of ceramic tiles using gray-based response surface methodology. *Arab. J. Sci. Eng.* **40**, 3299–3311 (2015)
 23. Santhanakumar, M.; Adalarasan, R.; Siddharth, S.; Velayudham, A.: An investigation on surface finish and flank wear in hard machining of solution treated and aged 18% Ni maraging steel. *J. Braz. Soc. Mech. Sci. Eng.* **39**, 2071–2084 (2017)
 24. Adalarasan, R.; Sundaram, A.S.: Parameter design in friction welding of Al/SiC/Al₂O₃ composite using gray theory-based principal component analysis (GT-PCA). *J. Braz. Soc. Mech. Sci. Eng.* **37**, 1515–1528 (2015)
 25. Kumar, R.; Balasubramanian, M.: Application of response surface methodology to optimize process parameters in friction welding of Ti–6Al–4V and SS304L rods. *T. Nonferr. Metal. Soc.* **25**, 3625–3633 (2015)
 26. Kadaganchi, R.; Gankidi, M.R.; Gokhale, H.: Optimization of process parameters of aluminum alloy AA 2024-T3 friction stir welds by response surface methodology. *Def. Technol.* **11**(3), 209–219 (2015)
 27. Adalarasan, R.; Santhanakumar, M.; Thileepan, S.: Selection of optimal machining parameters in pulsed CO₂ laser cutting of Al6061/Al₂O₃ composite using Taguchi-based response surface methodology (T-RSM). *Int. J. Adv. Manuf. Technol.* **93**(1–4), 305–317 (2016)
 28. Mohan Kumar, S.; Sankarapandian, S.; Siva Shanmugam, N.: Investigations on mechanical properties and microstructural examination of activated TIG-welded nuclear grade stainless steel. *J. Braz. Soc. Mech. Sci. Eng.* **42**, 292 (2020)
 29. Dhandha, K.H.; Badheka, V.J.: Comparison of mechanical and metallurgical properties of modified 9Cr–1Mo steel for conventional TIG and A-TIG welds. *Trans. Indian Inst. Met.* **72**, 1809–1821 (2019)
 30. Atcharawadi, T.; Boonruang, C.: Design of boiler welding for improvement of lifetime and cost control. *Materials.* **9**(11), 891–906 (2016)

